Proc. Indian Acad. Sci. (*Chem. Sci.*), Vol. 115, Nos 5 & 6, October–December 2003, pp 649–661

Preparation structure and dielectric behaviour of the system $Sr_{1-x}La_xTi_{1-x}Fe_xO_3$ ($x \leq 0{\cdot}50$)¶

OM PARKASH[1]*, DEVENDRA KUMAR[1] and C C CHRISTOPHER[2]
[1]Department of Ceramic Engineering, Banaras Hindu University, Varanasi 221 005, India
[2]School of Materials Science and Technology, Institute of Technology, Banaras Hindu University, Varanasi 221 005, India
e-mail: oparkash@banaras.ernet.in

Abstract. Formation of solid solution has been explored in the valence compensated perovskite oxide system $Sr_{1-x}La_xTi_{1-x}Fe_xO_3$ ($x \leq 0{\cdot}50$). XRD studies indicate the formation of solid solution for the whole range investigated. All the compositions synthesised have cubic structure similar to undoped $SrTiO_3$. Study of dielectric behaviour of these materials show that orientational polarisation and space charge polarisation contribute significantly to it.

Keywords. Perovskite oxide; strontium titanate; lanthanum ferrite dielectric behaviour.

1. Introduction

Alkaline earth titanates of general formula $MTiO_3$ (M = Ca, Sr, Ba and Pb) and having perovskite structure are useful materials because of their wide applications in the electronics industry. Owing to their ferroelectric and piezoelectric properties, $BaTiO_3$ and $PbTiO_3$ form the basis of a variety of electronic devices. Besides its relevance for electronics, sensor science, electrochemistry and photochemistry, $SrTiO_3$ is an excellent model material for a mixed type conductor because of availability of a detailed knowledge of its defect models, chemical and transport parameters. $SrTiO_3$ is paraelectric at room temperature and doesn't posses any interesting dielectric properties in undoped form.[1]

In recent years strontium titanate has attracted much attention due to its fascinating properties. Compositional modification in $SrTiO_3$ alters its properties and promotes its use in electronic devices.[2,3] Donor doped polycrystalline strontium titanate exhibits interesting and useful dielectric properties. Donor doping influences the electrical properties of $SrTiO_3$ mainly by increasing the volatility of oxygen from the grains during sintering, and by decreasing the rate of re-oxidation during cooling.[4] Semiconducting strontium titanate obtained by heating donor doped material in atmospheres of low oxygen content is used as a basis for manufacturing boundary layer capacitors.[2,5,6] Acceptor doped $SrTiO_3$ is photochromic,[7] electrochromic[8,9] and can be used for sub-millimetre MASER applications.[10]

¶Dedicated to Professor C N R Rao on his 70th birthday
*For correspondence

$LaFeO_3$ is a semiconductor and has wide technological applications such as solid oxide fuel cells, CO and NO_2 sensors.[11–14] Although significant work has been done on La- and Fe-doped $SrTiO_3$, to the best of our knowledge, the effect of simultaneous substitution of La^{3+} on Sr^{2+} site and Fe^{3+} on Ti^{4+} site in $SrTiO_3$ has not been reported so far. This simultaneous substitution of a donor (La^{3+}) the on A (Sr^{2+}) site and an acceptor (Fe^{3+}) on the B (Ti^{4+}) site in equal concentration leads to formation of so-called valence-compensated solid solution. The charge neutrality is maintained internally without creating any vacancies in A, B or O sub-lattices. Analogous valence-compensated $SrTiO_3$ doped with $LaCoO_3$ system exhibits dielectric relaxor-like behaviour with a very high value of dielectric constant, characteristic of barrier layer materials.[15] They exhibit barrier layer characteristics even on sintering in air at a considerably low temperature, i.e. 1300–1350°C.[16] This kindled our interest in investigating the possibility of formation of the solid solution $Sr_{1-x}La_xTi_{1-x}Fe_xO_3$ and investigating its dielectric properties. In this paper, we have restricted our studies to Sr-rich region i.e. ($x \leq 0{\cdot}50$) because of our interest in dielectric properties.

2. Experimental

Attempts were made to prepare samples with compositions $x = 0{\cdot}01$, $0{\cdot}03$, $0{\cdot}05$, $0{\cdot}10$, $0{\cdot}20$, $0{\cdot}30$ and $0{\cdot}50$ by conventional solid state ceramic route. All the samples were prepared using reagent grade chemicals (purity > 99·5) namely strontium carbonate, lanthanum oxalate, titanium dioxide and iron oxide. As the water of hydration of lanthanum oxalate depends on the conditions of its precipitation, lanthanum oxalate was estimated as lanthanum oxide for the purpose of batch calculations. A known quantity of lanthanum oxalate taken in a previously dried and weighed platinum crucible was heated at 1273 K for 4 h. Then, the platinum crucible was removed after cooling the furnace to 873 K and kept in a descicator till it cooled to room temperature. The platinum crucible was weighed quickly to avoid any water absorption. Lanthanum oxalate was estimated as lanthanum oxide.

Stoichiometric amounts of various chemicals mentioned above were accurately weighed and mixed in a ball mill for six hours using acetone as a medium. The mixed powders were dried and calcined at 1473 K for 24 h in a covered platinum crucible. The calcined powders were ground and mixed with appropriate quantities of 2% solution of polyvinyl alcohol as binder. These powders were pressed as cylindrical pellets having thickness in the range 0·1–0·2 cm and diameter 1·2 cm using a hydraulic press.

The pellets of each composition were kept in a platinum crucible and heated slowly to 873 K and maintained at this temperature for about an hour to burn off the binder completely. Thereafter, the temperature was raised to a required firing temperature (1623 K) at which both sintering as well as solid state reaction amongst various constituents takes place. These pellets were maintained at their respective firing temperatures for sufficiently long duration (24 h). After firing, the furnace was cooled at the rate of 3°C per minute up to 873 K and then switched off. The samples were then examined using X-ray diffraction to confirm the formation of single-phase materials.

The sintered pellets were ground and powder X-ray diffraction patterns were recorded using X-ray diffractometer (Rigaku Rotaflex RTP 300) employing Cu-K_{a1} radiations with a Ni filter. Capacitance and dielectric loss were measured in the frequency range 10 Hz to 1 MHz, at different steady temperatures using an impedance analyser (Hewlett

Packard 4192A LF). Measurements were repeated at least on two pellets to examine the reproducibility of the obtained results.

3. Results and discussion

The formation of single-phase solid solution was confirmed by the absence of characteristic lines of constituent oxides or any compounds between them in their XRD patterns. The diffraction patterns of the various compositions with $x = 0.01$, 0·03, 0·05, 0·10, 0·20, 0·30 and 0·50 could be indexed on the basis of a cubic unit cell similar to undoped strontium titanate. The lattice parameters for all the compositions determined using least square fitting of the data are given in table 1.

From table 1 it is observed that lattice parameter remains almost constant up to $x = 0.10$ and increases thereafter. This can be understood in terms of ionic radii of Sr^{2+} (1·44 Å), La^{3+} (1·32 Å), Ti^{4+} (0·605 Å) and Fe^{3+} (0·645 or 0·55 Å) depending on whether it exists in high or low spin state respectively).[17] Since the ionic radii of La^{3+} is less than that of Sr^{2+}, it is expected that the lattice parameter should decrease with increase in x. But, for the lower values of x, i.e. $x \leq 0.10$, the lattice parameter remains almost constant. This may be due to the formation of Fe^{2+} ions for $x > 0.10$ as mentioned below.

Due to high temperature sintering of these samples, depending on the thermodynamic conditions, oxygen may leave the lattice, leaving behind oxygen vacancies. At temperatures above 875 K, they are doubly ionised, $V_O^{\bullet\bullet}$.

$$O_O^x \Leftrightarrow V_O^{\bullet\bullet} + 2e' + \tfrac{1}{2}O_2. \tag{1}$$

Here all the species are written in accordance with Kröger Vink notation of defects. The electrons released in this reaction may be captured by Fe^{3+} ions to form Fe^{2+} ions. These Fe^{2+} ions are in high spin state having ionic radii of 0·78 Å.[18] For the lower values of x i.e. $x \leq 0.10$, Fe^{2+} ions are in small amount which compensates the decrease in lattice parameter thus making it to remain almost constant. The concentration of Fe^{2+} ions increases with increase in x. For $x > 0.10$, the increase in concentration of Fe^{2+} ions is more than required to compensate the decrease in the lattice parameter due to the La^{3+} ions and thus there is increases the lattice parameter with increase in x.

Density of the sintered specimens was determined from the geometrical dimensions and the mass of the pellets. X-ray or theoretical densities were calculated from the lattice parameter and the molecular weight of the samples. It is noted from table 1 that the

Table 1. Lattice parameters, theoretical density, experimental density, and % porosity of all the compositions prepared in the system $Sr_{1-x}La_xTi_{1-x}Fe_xO_3$.

Composition 'x'	Lattice parameter (Å) (± 0·001)	Experimental density (g/cc)	Theoretical density (g/cc)	% Porosity
0·01	3·907	4·97	5·24	4·8
0·03	3·908	4·99	5·26	5·1
0·05	3·907	5·02	5·29	5·2
0·10	3·909	5·08	5·36	5·3
0·20	3·912	5·20	5·50	5·5
0·30	3·922	5·32	5·64	5·6
0·50	3·928	5·59	5·93	5·7

density increases with increasing x. This can be understood in terms of the atomic weights of the dopants with respect to the host ions. When Sr^{2+} (at. wt. 87·6) is replaced by La^{3+} (at. wt. 138·9) and Ti^{4+} (at. wt. 47·9) is replaced by Fe^{3+} (at. wt. 55·85), owing to the difference in the atomic weights of the dopants and the host ions, the density increases. The % porosity of various compositions prepared in these systems lies in the range 4–6%.

Dielectric constant and dielectric loss were measured as a function of temperature (300–550 K) and frequency (10 Hz–1 MHz). The variation of dielectric constant, ε_r, and dissipation factor, D, with temperature, for a few typical compositions at 1, 10 and

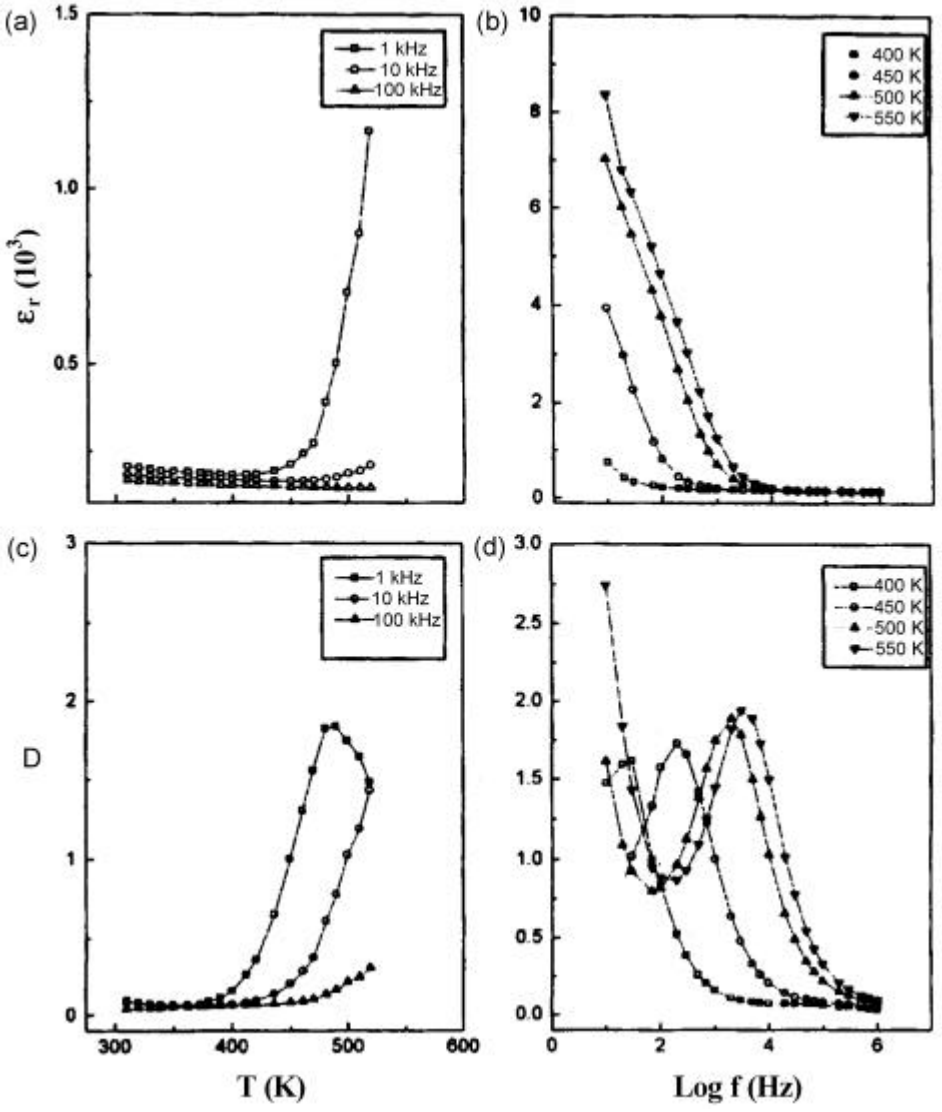

Figure 1. Variation of (**a**) ε_r with temperature, (**b**) ε_r with frequency, (**c**) D with temperature, and (**d**) D with frequency for the composition $Sr_{0.99}La_{0.01}Ti_{0.99}Fe_{001}O_3$.

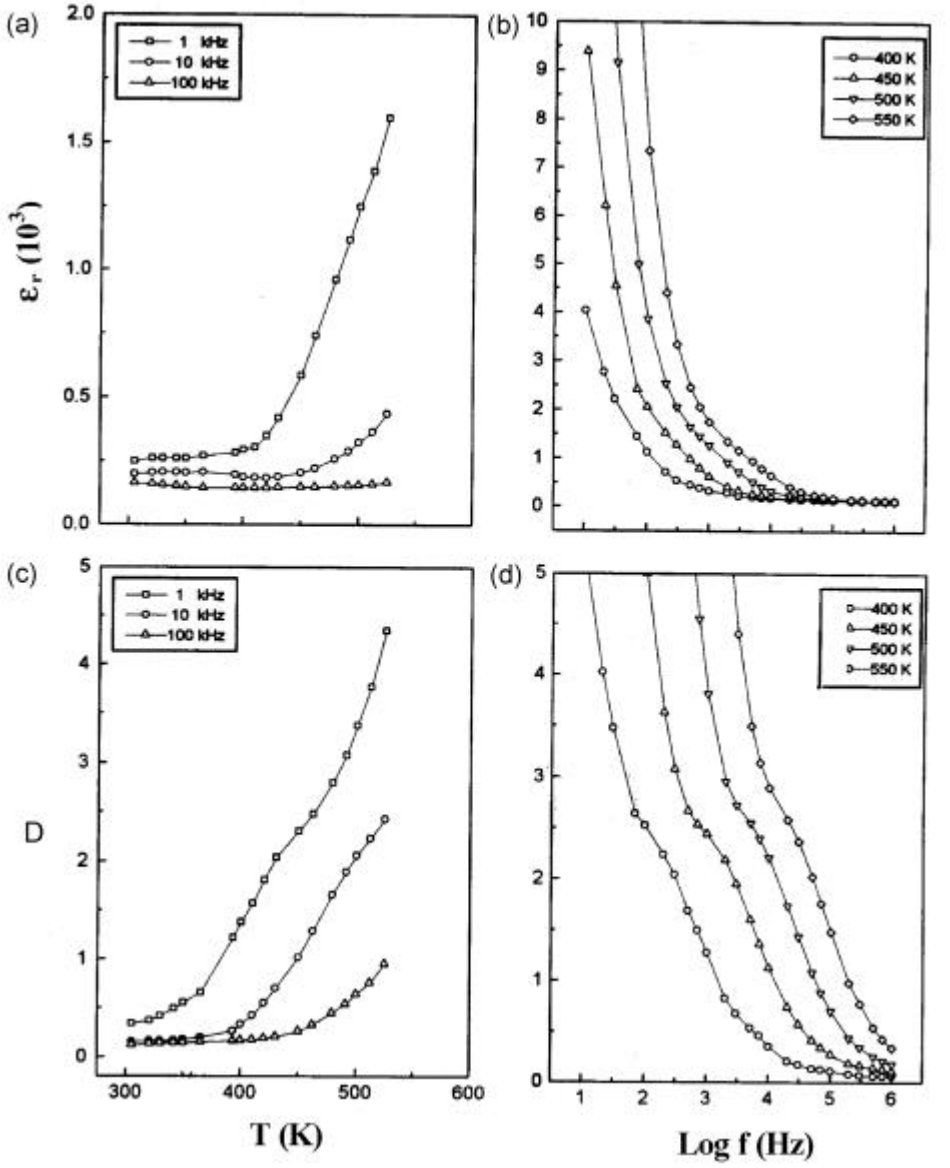

Figure 2. Variation of (**a**) ε_r with temperature, (**b**) ε_r with frequency, (**c**) D with temperature, and (**d**) D with frequency for the composition $Sr_{0.90}La_{0.10}Ti_{0.90}Fe_{0.10}O_3$.

100 kHz is given in the figures 1(a, c)–3(a, c) respectively. The behaviour of the compositions with $x \leq 0.10$ is similar. Both ε_r and D remain constant up to a particular temperature and thereafter increase rapidly with increasing temperature. The temperature dependence of ε_r and D becomes less pronounced with increasing frequency. Further, both these parameters decrease with increasing frequency. The dielectric constant increases with x, at first slowly up to $x = 0.05$ and rapidly thereafter. Dissipation factor,

D, remains almost constant up to $x = 0{\cdot}05$ and then increases rapidly. This seems to be due to increase in conductivity with increasing x.

Samples with compositions $x = 0{\cdot}20$, $0{\cdot}30$ and $0{\cdot}50$ exhibit an anomaly in the ε_r vs T plots which shifts to higher temperature with increasing frequency. The peak value of ε_r decreases with increasing frequency. A peak is observed in D vs T plots also for these compositions. These features show that these materials mimic relaxor ferroelectrics.

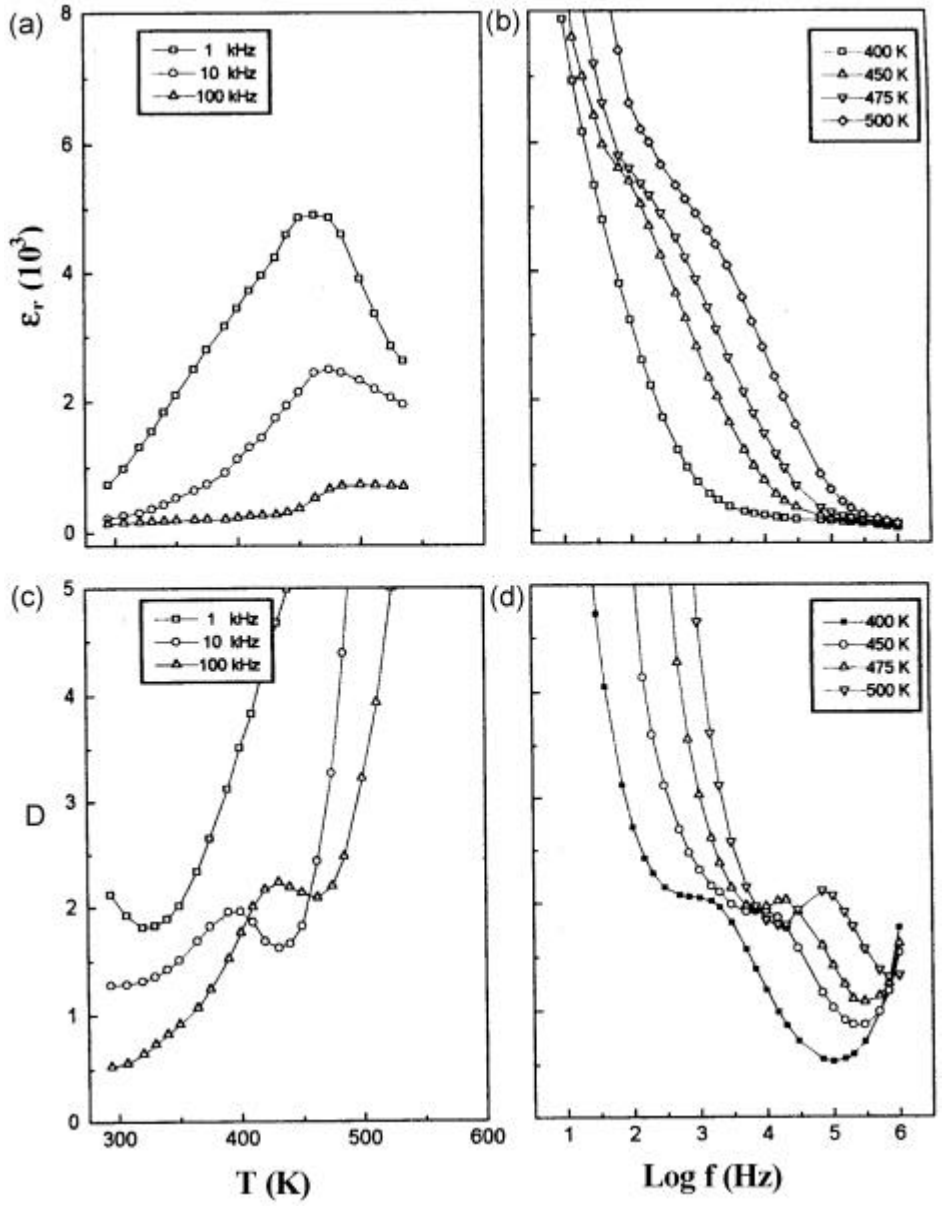

Figure 3. Variation of (**a**) ε_r with temperature, (**b**) ε_r with frequency, (**c**) D with temperature, and (**d**) D with frequency for the composition $Sr_{0{\cdot}50}La_{0{\cdot}50}Ti_{0{\cdot}50}Fe_{0{\cdot}50}O_3$.

The variation of dielectric constant and loss D with frequency at different temperatures for some compositions are given in the figures 1(b, d)–3(b, d). ε_r decreases rapidly with increasing frequency. In all the compositions, Debye-type relaxation is clearly observed in the intermediate frequency range. This is also reflected in the D vs log f plots. The peaks observed in the D vs log f plots shift to higher frequency region with increase in temperature. For the compositions with $x = 0{\cdot}05$ and $0{\cdot}10$, the peaks are not well resolved. From the peak maxima of the D vs log f plots, the relaxation time τ_D was calculated using the relation $\omega\tau_D = 1$. Here ω is the angular frequency, which is equal to $2\pi f_{max}$ and τ_D is the relaxation time for the polarisation process involved. With the increase in temperature, τ_D decreases and therefore the relation $\omega\tau_D = 1$ is satisfied at higher frequencies. This is why the peaks shift to higher frequency region with increase in temperature. Log τ_D is plotted as a function of $1000/T$ in the figure 4a. These plots are linear, showing τ_D follows the relation,

$$\tau_D = \tau_0 \exp(E_D / RT), \tag{2}$$

where E_D is the activation energy for the relaxation process. The activation energies calculated by the least squares fitting of the data are given in table 2.

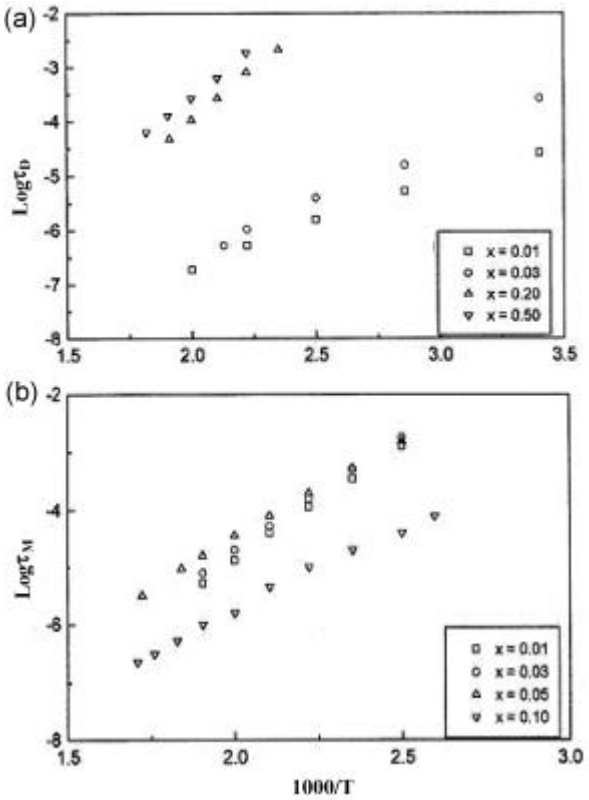

Figure 4. Plots of (**a**) log τ_D vs $1000/T$ and (**b**) log τ_M vs $1000/T$ for the system $Sr_{1-x}La_xTi_{1-x}Fe_xO_3$.

Table 2. Activation energy calculated from log t_D vs 1000/T (E_D) and log t_M vs 1000/T (E_M) plots for various compositions in the system $Sr_{1-x}La_xTi_{1-x}Fe_xO_3$.

Composition 'x'	E_D from log t_D vs 1000/T plots (eV)	E_M from log t_M vs 1000/T plots (eV)
0·01	0·75 ± 0·08	0·83 ± 0·06
0·03	0·72 ± 0·04	0·80 ± 0·04
0·05	–	0·68 ± 0·03
0·10	–	0·50 ± 0·01
0·20	0·40 ± 0·01	–
0·30	0·35 ± 0·01	–
0·50	0·31 ± 0·01	–

The system under present investigation is expected to contain associated defect pairs viz. $Fe'_{Ti^{4+}} - V_O^{\bullet}$ or $Fe''_{Ti^{4+}} - V_O^{\bullet\bullet}$. The origin of these dipoles can be explained as follows.

All the compositions in this system are sintered at high temperatures. Due to high temperature sintering, depending on the thermodynamic conditions, oxygen may leave the lattice, generating oxygen vacancies. At temperatures above 875 K, they are doubly ionised, $V_O^{\bullet\bullet}$ as given in (1). At lower temperatures, < 675 K, the oxygen vacancies become singly ionised, $V_O^{\bullet}$.[19–22] The change in ionisation can be written as:

$$V_O^{\bullet\bullet} + e' \Leftrightarrow V_O^{\bullet}. \tag{3}$$

These singly ionised oxygen vacancies are called intrinsic donors.[23] The electrons released in (1) and (3) may be captured by the Fe^{3+} ions to form Fe^{2+} ions. The presence of Fe^{4+} ions in the Fe doped $SrTiO_3$ has been reported in the literature.[24,25] Also it has been reported that the presence of La in $SrTiO_3$ facilitates the loss of oxygen from the crystal lattice.[4] In the present case, since La is codoped along with Fe in $SrTiO_3$, it facilitates the loss of oxygen thereby suppressing the formation of Fe^{4+} ions and promoting the formation of Fe^{2+} ions. Due to coulombic attraction, these Fe^{3+} and Fe^{2+} ions on Ti^{4+} sites may form dipoles with the oxygen vacancies, viz., $[Fe'_{Ti^{4+}} - V_O^{\bullet}]$ and $[Fe''_{Ti^{4+}} - V_O^{\bullet\bullet}]$ respectively. These dipoles may change their orientation due by hopping of electrons among Fe^{2+}–Fe^{3+} sites. The peaks observed in D vs T and D vs log f plots, are due to the relaxation of this orientational polarisation. The value of activation energy decreases systematically with increasing x. This is due to the increase in the concentration of Fe^{2+} ions with increase in x leading to increased concentration of such associated defect pairs.

It is noted that the relaxational peaks for a few compositions in this system are not well resolved in the D vs log f plots in the frequency and the temperature range investigated. The relaxational peaks due to the same polarisation process appear at different frequencies in spectroscopic plots of different immittance functions, i.e. in M'' vs log f, Z'' vs log f, ϵ' vs log f and Y'' vs log f plots, where M'', Z'', ϵ' and Y'' represent the imaginary parts of total modulus, total impedance, total susceptance and total admittance respectively.[26] The four immittance functions are related to each other and the dissipation factor, D, through the following equations:

$$M^* = M' + jM'' = \frac{1}{\epsilon^*}, \tag{4}$$

$$Z^* = Z' - jZ'' = \frac{1}{jwC_0\varepsilon^*}, \tag{5}$$

$$\varepsilon^* = \varepsilon' - j\varepsilon'' \text{ and } k^* = \frac{\varepsilon^*}{\varepsilon_0}, \tag{6}$$

$$D = \frac{\varepsilon''}{\varepsilon'} = \frac{M''}{M'} = \frac{Z'}{Z''} = \frac{Y'}{Y''}. \tag{7}$$

In order to study the relaxational polarisation in the compositions which do not show peaks in their D vs log f plots, the immittance data are presented as modulus spectroscopic plots. M'' vs log f plots of a few compositions at some selected temperatures are shown in figures 5–7. A broad peak is observed in the compositions $x = 0{\cdot}10$. As x

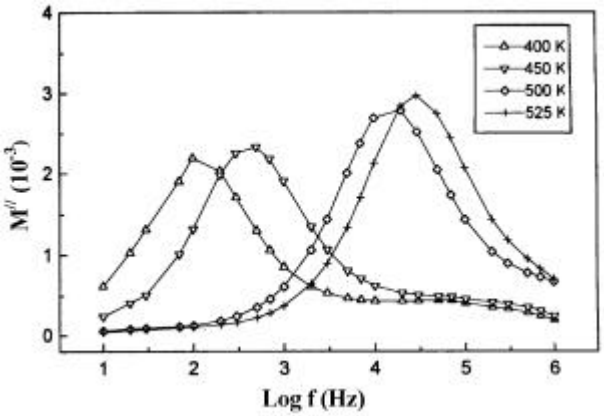

Figure 5. Plots of M'' vs log f for the composition, $Sr_{0{\cdot}99}La_{0{\cdot}01}Ti_{0{\cdot}99}Fe_{0{\cdot}01}O_3$.

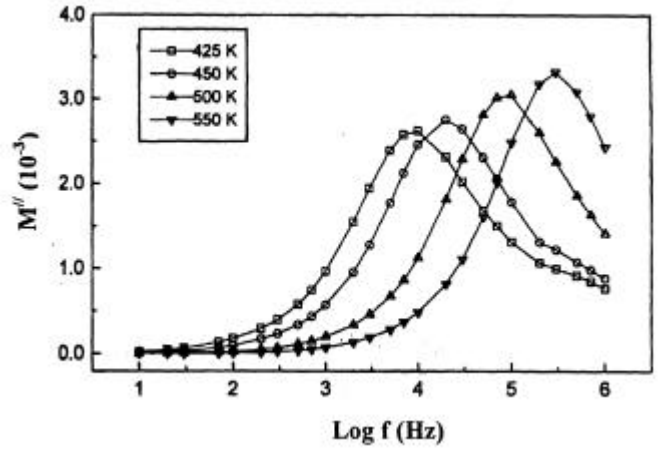

Figure 6. Plots of M'' vs log f for the composition, $Sr_{0{\cdot}90}La_{0{\cdot}10}Ti_{0{\cdot}90}Fe_{0{\cdot}10}O_3$.

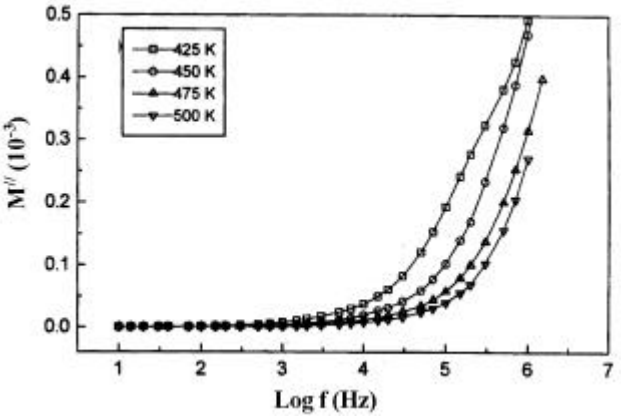

Figure 7. Plots of M'' vs log f for the composition, $Sr_{0\cdot50}La_{0\cdot50}Ti_{0\cdot50}Fe_{0\cdot50}O_3$.

increases, the peak shifts to higher frequencies. For $x = 0\cdot30$ and $0\cdot50$, the peaks appear to shift to higher frequencies beyond the range of the measurements. One common feature of the M'' vs log f plots is that the peak height increases and the f_{max} shifts to higher frequency with increase in temperature. As x increases, broadness of the peak increases and the position of the peak shifts to higher frequency. All the peaks observed are not ideal Debye peaks i.e. full width at half maxima (FWHM) is more than 1·14 decades. From the peak maxima of M'' vs log f plots for the various compositions, the relaxation times τ_M are calculated. Plots of log τ_M vs $1000/T$ (figure 4b) are linear showing that the relaxation time obeys the Arrhenious relation:

$$\tau_M = \tau_0 e_M^{-E} / KT, \tag{8}$$

where E_M is the activation energy of the relaxation process. The values of activation energy calculated from the slopes of these plots by least square fitting of the data are given in table 2. The activation energy obtained from these plots is comparable with that obtained from log τ_D vs $1000/T$ plots. This shows that the relaxation peaks in M'' vs log f and D vs log f has the same origin i.e. due to the dipole formation and their reorientation as explained earlier. With increasing x, the probability of forming associated defect pairs increases. This facilitates the reorientation of dipoles either through hopping of electrons between Fe^{2+} and Fe^{3+} sites or by jumping of oxygen vacancies around the FeO_6 octahedra. This leads to decrease in the value of activation energy of relaxation as observed experimentally.

Strong dispersion is observed in the values of ε_r in the frequency range 10 Hz to 10 kHz for compositions up to $x \leq 0\cdot10$. For compositions with $x > 0\cdot10$, the dispersion seems to occur in the range 10 Hz to 1 MHz with steep rise in ε_r at low frequencies. The dispersion decreases with increase in frequency for all the compositions. A peak is observed in D vs log f plots of all the compositions. These peaks are displaced on the frequency scale relative to the inflection point observed in ε_r vs log f plots. These features clearly show that two polarisation mechanisms are active in this system.

In ceramic materials, polarisation occurs by four primary mechanisms. Each polarisation involves a short range motion of charge and contributes to the total polarisation.

The four primary polarisation mechanisms are; (i) Electronic polarisation, (ii) atomic polarisation, (iii) dipole or dipolar polarisation, and (iv) interfacial polarisation. Electronic and atomic polarisations are active up to 10^{12} Hz, which is beyond the scope of the present study. Dipole or dipolar polarisation is also referred to as orientation polarisation involves the perturbation of the thermal motion of ionic or molecular dipoles, producing a net dipolar orientation in the direction of the applied field. The dipolar polarisation is of two types. In the first type, the molecules containing permanent dipole moment may be rotated against an elastic restoring force about an equilibrium position. The frequency response for this type of dipolar polarisation is of the order of 10^{11} Hz at room temperature and is known to operate in a variety of liquids, gases and polaroid solids. The second type comprising the rotation of dipoles between two equivalent equilibrium positions is important in the dielectric behaviour of glasses and ceramics. Since appreciable distance is involved in the oscillation or the rotation of the dipoles, the polarisation occurs within a range of frequency between 10^3–10^6 Hz. The fourth and the last mechanism of polarisation is the interfacial polarisation or the space charge polarisation, which arises whenever mobile charge carriers are obstructed by a physical barrier inhibiting their motion. The obstructed charges pile up at the barrier producing a localised polarisation. When AC fields of sufficiently low frequencies i.e. $< 10^3$ Hz are applied, the oscillation of charges between barriers which are far apart occurs, leading to very high value of dielectric constant. If the barriers encountered by the mobile charge carriers are the internal structural features of the ceramic, the frequency range of interfacial polarisation extend into kilo cycles.[27] In this case it is impossible to distinguish the frequency response of a dipolar mechanism from that of an interfacial polarisation mechanism.

All the features mentioned above from the variation of dielectric constant and loss *D* with temperature and frequency plots show that the dielectric behaviour in these systems is predominantly due to space–charge polarisation at lower frequency. The space–charge polarisation arises whenever two or more phases with different electrical conductivity are present in the different regions of the same sample.[28] The present samples are prepared by diffusion controlled solid state ceramic method. The grain-boundaries are the regions of micro-heterogeneities in these samples. There is a difference in electrical conductivity between the grains and grain-boundaries. The grain-boundaries are relatively insulating and give rise to interfacial polarisation. The low frequency shoulder observed for all the

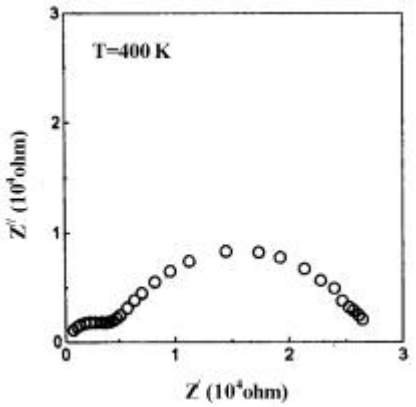

Figure 8. Plots of *Z″* vs *Z′* at 400 K for the composition, $Sr_{0·80}La_{0·20}Ti_{0·80}Fe_{0·20}O_3$.

compositions in the ε_r vs log f plots may be due to space charge polarisation. The peaks observed in the D vs log f plots for all the compositions and strong dispersion seen in the frequency range 1 kHz to 1 MHz may be due to the dipolar polarisation. Dipolar polarisation arises because of the formation of dipoles as mentioned earlier. For compositions with $x \leq 0{\cdot}10$, it seems impossible to differentiate the dipolar polarisation from space–charge polarisation due to the reasons stated above.

It is also noted that ε_r vs T plots for compositions with $x > 0{\cdot}10$ show a broad peak with high values of dielectric constant. It has been reported that, the samples in the system. $Sr_{1-x}La_xTi_{1-x}Co_xO_3$ with $0{\cdot}10 \leq x \leq 0{\cdot}40$ exhibit a diffused peak in the ε_r vs T plots with high value of dielectric constant, which is characteristic of barrier layer capacitors.[16] The high values of dielectric constant in compositions $x \geq 0{\cdot}20$ in this system may be attributed to the formation of barrier layers at grain–grain-boundaries interfaces similar to the analogous system. $Sr_{1-x}La_xTi_{1-x}Co_xO_3$. For example, the complex plane impedance plot at 400 K for the composition with $x = 0{\cdot}20$ is shown in figure 8. Two semicircular arcs are clearly visible in the above figure. The arc passing through the origin may be assigned to grain contribution and the second arc, on the lower frequency side, may be assigned to grain boundary contribution to the total resistance of the sample.[29] The resistance values are obtained from the intercepts, which the two arcs make on the x-axis. From the resistance values obtained, it was found that the contribution of grains and grain-boundaries to the total resistance of the sample are $4{\cdot}58 \times 10^3$ and $17{\cdot}14 \times 10^3\ \Omega$ respectively. If we assume the grain-boundaries to be $0{\cdot}01\ \mu$m thick, the ratio of the resistivity of the grain-boundaries to the grains would be (taking average grain size to be $2\ \mu$m) $2 \times 22{\cdot}4 \times 10^3/0{\cdot}01 \times 4{\cdot}59 \times 10^3 = 976$. Hence the grain-boundaries are much more resistive as compared to the bulk of the sample confirming the formation of barrier layers in these materials.

4. Conclusion

Solid solutions form in the system $Sr_{1-x}La_xTi_{1-x}Fe_xO_3$ over the full range investigated in the present work, i.e. for $x \leq 0{\cdot}50$. All the compositions synthesised have cubic structure, small grain size with % porosity less than 6%. The dielectric behaviour of all the samples synthesised shows that both interfacial and dipolar polarisations contribute to their dielectric character. The high values of dielectric constant in the compositions with $x \geq 0{\cdot}20$ may also be attributed to the formation of barrier layers at grain–grain-boundaries interfaces which is revealed through complex plane impedance analysis.

Acknowledgements

Financial support from the Department of Science and Technology, Government of India, New Delhi, is gratefully acknowledged. The authors are thankful to Mr L K Srivastava, Scientist, Research Design and Standard Organisation, Lucknow and Prof D Pandey, Co-ordinator, School of Materials Science and Technology, Institute of Technology, Banaras Hindu University, Varanasi for extending the SEM and XRD facilities respectively.

References

1. Mitsui T and Westphal W B 1961 *Phys. Rev.* **124** 1354
2. Waku S 1967 *Rev. Elect. Commun. Lab.* **15** 689
3. Yamaoka N, Masuyama M and Fukui M 1983 *Bull. Am. Ceram. Soc.* **62** 698

4. Burn I and Neirman S 1982 *J. Mater. Sci.* **17** 3510
5. Takahashi Y, Yamaoka N, Yamaoka Y and Kakubari S 1976 *US Patent* 3 933688
6. Itakura G and Iguchi T 1979 *US Patent* 4143, 207
7. Faughan B W 1971 *Phys. Rev.* **B4** 3623
8. Blanc J and Stabler D L 1971 *Phys. Rev.* **B4** 3548
9. Mohapatra S L and Wagner S 1979 *J. Appl. Phys.* **50** 5001
10. Kirkpatrick E S, Muller K A and Rubins R S 1964 *Phys. Rev.* **135** A86
11. Li W B, Yoneyama H and Tamura H 1982 *Nippon Kagaku Kaishi* 761
12. Minh N Q 1993 *J. Am. Ceram. Soc.* **76** 563
13. Matsuura Y, Matsushima S, Sakamoto M and Sadaoka Y 1993 *J. Mater. Chem.* **3** 767
14. Traversa E, Matsushima S, Okada G, Sadaoka Y, Sakai Y and Watanabe K 1995 *Sens. Actuators* **B25** 661
15. Parkash O, Prasad C D and Kumar D 1989 *J. Mater. Sci. Lett.* **8** 385
16. Parkash O, Prasad C D and Kumar D 1990 *J. Mater. Sci.* **25** 487
17. Shannon R D and Prewitt C T 1969 *Acta Crystallogr.* **B25** 925
18. Shannon R D and Prewitt C T 1970 *Acta Crystallogr.* **B26** 1046
19. Gerthsen K H, Hardtl and Csillag A 1972 *Phys. Status Solidi* **A13** 127
20. Lee C, Destry J and Brebner L J 1975 *Phys. Rev.* **B11** 2299
21. Moos R, Gnudi A and Hardtl K H 1995 *J. Appl. Phys.* **78** 5042
22. Moos R, Menesklou and Hardtl K H 1995 *J. Appl. Phys.* **A61** 389
23. Moos R and Hardtl K H 1997 *J. Am. Ceram. Soc.* **80** 2549
24. Clevenger Jr T R 1963 *J. Am. Ceram. Soc.* **46** 207
25. Zhuang Y, Lin Y, Zhu D, Zheng Y and Yu Z 1989 *J. Am. Ceram. Soc.* **72** 1444
26. Gerhardt R 1994 *J. Phys. Chem. Solids* **55** 1491
27. Hench L L and West J K 1989 *Principles of electronic ceramics* (New York: John Wiley and Sons) p. 47
28. Jonscher A K 1983 *Dielectric relaxation in solids* (London: Chelsea Dielectric Press)
29. Glaister R M and Woolmer J W 1959 *J. Electr. Control* **6** 385